PHYSICAL REVIEW E **79**, 030904(R) (2009)

Diffusion in narrow domains and application to phototransduction

Jürgen Reingruber
Department of Computational Biology, Ecole Normale Supérieure, 46 rue d'Ulm, 75005 Paris, France

David Holcman
Department of Applied Mathematics, Weizmann Institute of Science, Rehovot 76100, Israel
and Department of Computational Biology, Ecole Normale Supérieure, 46 rue d'Ulm, 75005 Paris, France

(Received 2 June 2008; revised manuscript received 2 December 2008; published 17 March 2009)

The mean time for a Brownian particle to find a small target inside a narrow domain is a key parameter for many chemical reactions occurring in cellular microstructures. Although current estimations are given for a large class of domains, they cannot be used for narrow domains often encountered in cellular biology, such as the synaptic cleft, narrow compartments in the outer segment of vertebrate photoreceptors, or neuron-glia contact. We compute here the mean time for a Brownian particle to hit a small target placed on the surface of a narrow cylinder. We then use this result to estimate the rate constant of cyclic-GMP (cGMP) hydrolysis by the activated enzyme phosphodiesterase (PDE) in the narrow microdomains that build up the outer segment of a rod photoreceptor. By controlling the cGMP concentration, PDE activity is at the basis of the early photoresponse chemical reaction cascade. Our approach allows us to compute the cGMP rate constant as a function of biophysical parameters.

DOI: 10.1103/PhysRevE.79.030904 PACS number(s): 87.16.A−, 87.16.Xa, 87.14.ej

The mean time for a Brownian particle to reach a small target located on a surface of a microdomain is ubiquitous in cellular biology, because it represents the reciprocal of the forward binding rate [1–3]. Recent numerical and analytical approaches lead to precise estimates [4–8] of the narrow escape time (NET) in a confined geometry. These computations were further generalized to the case of several targets [9] and also to stochastic dynamics with a potential well [10,11]. However, the usual narrow escape formulas are not valid for degenerated microdomains where one of the dimensions is much smaller than the others. We recall that in a three-dimensional volume V with isoperimetric ratio of order 1, the NET through an absorbing circular target of radius a is in first order given by (D is the diffusion constant) $\tau = |V|/(4aD)$ [4,6,8]. The first goal of this article is to generalize this formula to narrow domains. There are indeed many cellular microdomains where one dimension is much smaller than the others: the geometry of the neuronal synaptic cleft can be approximated by a narrow cylinder [12] surrounded by glial cells. Synaptic transmission depends on the mean time neurotransmitter molecules find a functional receptor. Another example that we will study here in detail concerns the outer segment of rod and cone photoreceptors containing a stack of piled narrow cylinders. Photoreceptors become hyperpolarized after photon absorption, and this electrical response depends crucially on several chemical steps, limited by the rate constant by which the cytoplasmic diffusible cyclic GMP (cGMP) molecules, gating ionic membrane channels, are hydrolyzed by activated phosphodiesterase (PDE). We will use our new NET result in a narrow domain to estimate this rate constant.

We start by providing a formula for the mean first passage time (MFPT) $\tau(\boldsymbol{x})$ a Brownian molecule, starting at position $\boldsymbol{x}$ and confined in a thin cylinder of radius R and height l (Fig. 1), finds a small circular target of radius a located centrally on the bottom surface. A similar problem was also treated in [13] when studying an immunoassay reaction between diffusing ligands and immobile receptors gathered at a central spot of a surface. It is well known that $\tau(\boldsymbol{x})$ satisfies the mixed boundary-value problem [14]

$$D\,\Delta\tau(r,z) = -1, \quad 0 < z < l, \quad 0 \leqslant r < R,$$

$$\tau(r,z) = 0, \quad z = 0, \quad r \leqslant a,$$

$$\frac{\partial}{\partial z}\tau(r,z) = 0, \quad z = 0, \quad r > a, \quad z = l,$$

$$\frac{\partial}{\partial r}\tau(r,z) = 0, \quad r = R. \tag{1}$$

Using the scaled variables $x=r/a$, $y=z/a$, and $|\Omega|=|V|/a^3$ and the parameters $\alpha=R/a$ and $\beta=l/a$, the scaled MFPT

$$\hat{\tau}(x,y) = \frac{aD}{|V|}\tau(r,z) \tag{2}$$

can be determined by solving Eq. (1) in the domains $\Omega_i = \{x \mid x \leqslant 1\}$ and $\Omega_o = \{x \mid 1 \leqslant x \leqslant \alpha\}$, and matching the solutions at $x=1$. A general solution $\hat{\tau}_o(x,y)$ of Eq. (1) in Ω_o is

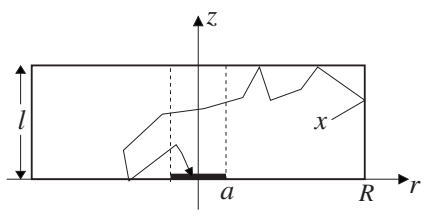

FIG. 1. NET in a narrow cylindrical microdomain: a Brownian particle moving in the cylinder is reflected on its surface, except at a small circular target located centrally on the lower surface, where it is absorbed.

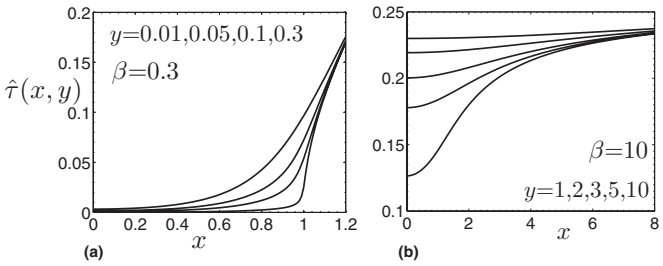

FIG. 2. NET as a function of the initial position. The graphs display $\hat{\tau}(x,y)$ [given by Eq. (6)] in the neighborhood of the absorbing disk for (a) $\beta=0.3$ and (b) $\beta=10$. By comparing panel (a) with (b) one can observe the evolution of the boundary layer around the absorbing disk (see also the explanations given in the text).

$$\hat{\tau}_o(x,y)=\sum_{n=0}^{\infty} a_n \frac{F_0(k_n x,k_n\alpha)}{F_0(k_n,k_n\alpha)}u_n(y)+\frac{\ln(x)}{2\pi\beta}-\frac{x^2-1}{4|\Omega|}, \quad (3)$$

with $k_n=n\pi/\beta$, $u_0=1/\sqrt{2}$, $u_n(y)=\cos(k_n y)$ $(n\geqslant 1)$, and $F_0(x,y)=I_0(x)K_1(y)+K_0(x)I_1(y)$ $(I_0,K_0,I_1,K_1$ are Bessel functions [15]). The last two terms in Eq. (3) are the two-dimensional solution to reach the boundary $x=1$ starting at $x>1$. Similarly, a solution $\hat{\tau}_i(x,y)$ in Ω_i is

$$\hat{\tau}_i(x,y)=\sum_{n=0}^{\infty} b_n \frac{I_0(l_n x)}{I_0(l_n)}v_n(y)+w_i(x,y), \quad (4)$$

with $l_n=(2n+1)\pi/(2\beta)$, $v_n(y)=\sin(l_n y)$, and

$$w_i(x,y)=\sum_{n=1}^{\infty} c_n \frac{J_0(z_n x)}{|\Omega|}\left(\frac{\cosh[z_n(\beta-y)]}{\cosh(z_n\beta)}-1\right), \quad (5)$$

where z_n are the positive zeros of the Bessel function J_0 and $c_n=[2J_0'(z_n)]^{-2}\int_0^1 J_0(z_n x)(x^2-1)x\,dx$. The unknown coefficients a_n and b_n in (3) and (4), respectively, are functions of α and β, and are specified by the compatibility conditions $\hat{\tau}_i(1,y)=\hat{\tau}_o(1,y)$ and $\frac{\partial}{\partial x}\hat{\tau}_i(1,y)=\frac{\partial}{\partial x}\hat{\tau}_o(1,y)$.

For $a\ll R$ $(\alpha\gg 1)$ the function $w_i(x,y)$ in Eq. (5) is of the order α^{-2} and can be neglected, and for $l\ll R$ $(\alpha/\beta\gg 1)$ we approximate $F_0(k_n x,k_n\alpha)/F_0(k_n,k_n\alpha)\approx K_0(k_n x)/K_0(k_n)$ $(k_n\alpha=n\pi\alpha/\beta)$. Equations (3) and (4) simplify to

$$\hat{\tau}(x,y)=\begin{cases}\displaystyle\sum_{n=0}^{\infty} b_n\frac{I_0(l_n x)}{I_0(l_n)}v_n(y), & (x,y)\in\Omega_i,\\ \displaystyle\sum_{n=0}^{\infty} a_n\frac{K_0(k_n x)}{K_0(k_n)}u_n(y)+\frac{\ln x}{2\pi\beta}-\frac{x^2-1}{4|\Omega|}, & (x,y)\in\Omega_o,\end{cases} \quad (6)$$

and from the compatibility conditions we obtain

$$b_n=\sum_{m=0}^{\infty}\xi_{nm}a_m, \quad \sum_{m=0}^{\infty}(\beta_n+\alpha_m)\xi_{nm}a_m=\gamma_0\xi_{n0}, \quad (7)$$

with the orthogonal matrix $\xi_{nm}=\frac{2}{\beta}\int_0^\beta v_n(y)u_m(y)dy$, $\alpha_n=k_n\frac{K_1(k_n)}{K_0(k_n)}$, $\beta_n=l_n\frac{I_1(l_n)}{I_0(l_n)}$, and $\gamma_0=\frac{1}{\sqrt{2}\pi\beta}$. Because Eq. (7) depends on β only, this parameter determines the behavior of the NET in narrow domains. To evaluate Eq. (6), we approximate numerically $a_n(\beta)$ and $b_n(\beta)$ in Eq. (7) by truncating the infinite sum at various levels (for example, for $\beta<1$ we use $\sim$40 coefficients and for $\beta\sim 10$ we use $\sim$200).

Using Eq. (6) we study the transition of the NET from a two- to a three-dimensional domain. For $\beta\to 0$ and $x>1$, Eq. (6) reduces to the two-dimensional radial solution $\hat{\tau}(x,y)=\ln x/(2\pi\beta)-(x2-1)/(4|\Omega|)$. For $\beta>0$, as depicted in Fig. 2, $\hat{\tau}(x,y)$ varies significantly only in a small boundary layer around the absorbing target [4,16,17], while outside this area $\hat{\tau}(x,y)$ changes slowly. For $\beta\gtrsim 10$, $\hat{\tau}(x,y)$ initially approaches the value $1/4$ outside the boundary layer [Fig. 2(b)], and the further behavior for large x depends on the ratio $\ln\alpha/\beta$: for $\ln\alpha/\beta\ll 1$, $\hat{\tau}(x,y)$ remains almost constant up to the lateral boundary, while for $\ln\alpha/\beta\gg 1$, $\hat{\tau}(x,y)$ increases $\sim\ln x$ for large x. Simulations (not presented here) reveal that the graph of $\hat{\tau}(x,y)$ in the neighborhood of the target for $\beta\gtrsim 10$ is almost identical to the one in Fig. 2(b) where $\beta=10$. From this, we conclude that the evolution of the boundary layer is completed when $\beta\sim 10$.

To obtain the expression for the NET τ in a narrow domain Ω with $\alpha\gg 1$ and $\alpha\gg\beta$, we average Eq. (6) over a uniform initial distribution and obtain

$$\tau=\frac{|V|}{aD}\left(\frac{a_0(\beta)}{\sqrt{2}}+\frac{4\ln\alpha-3}{8\pi\beta}\right). \quad (8)$$

The contributions to τ in Eq. (8) come only from $\hat{\tau}(x,y)$ in Ω_o because the volume $|\Omega_i|$ is by a factor α^2 smaller than $|\Omega_o|$, and hence the contribution from Ω_i is negligible, of order $\sim a_0(\beta)/\alpha^2$. The condition $\alpha\gg\beta$ is necessary to have $a_0(\alpha,\beta)\approx a_0(\beta)$, whereas the logarithm term (the two-dimensional part) does not rely on this condition. In Fig. 3 we plot $a_0(\beta)/\sqrt{2}$ as a function of β [obtained from Eq. (7)] together with results from Brownian simulations, which confirm the accuracy of our analysis. For large β, $a_0(\beta)/\sqrt{2}$ approaches $1/4$, and because the logarithm term in Eq. (8) is negligible for $\beta\gg\ln\alpha$, this is consistent with the NET formula $|V|/(4aD)$ for a three-dimensional spherical volume.

Although the first term in Eq. (8) was derived for $\beta\ll\alpha$, the asymptotic form $|V|/(4aD)$ for large β and the numerical results suggest that it remains valid up to $\beta\sim\alpha$, where the analytical and simulation values for $a_0(\beta)$ in Fig. 3 still agree very well. Nevertheless, in domains with $\beta\gg\alpha$ (these are no longer narrow domains), one needs to replace $a_0(\beta)$ with $a_0(\alpha,\beta)$. In this case, correction terms to Eq. (8) can be found by expanding $F_0(k_n x,k_n\alpha)/F_0(k_n,k_n\alpha)$ in Eq. (3) as a function of β/α; see also [18]. From Eq. (8) and Fig. 3 we find that the condition determining whether $|V|/(4aD)$ is a good approximation to the NET in an oblate volume, characterized by a radius α and a height β, is $\ln\alpha\ll\beta$, and not $\alpha\sim\beta$, as one might anticipate. As an example, for $\alpha=10^4$ and $\beta=50$, $|V|/(4aD)$ deviates from Eq. (8) only by around 10%. Finally, the position of the target does not affect the leading-order term of the NET: In dimension 2 (or $\beta\ll 1$) an off-centered disk can be mapped conformally to a centered disk and this mapping does not affect the leading-order term. In a three-dimensional volume, the leading-order term does also not depend on the position of the target [19].

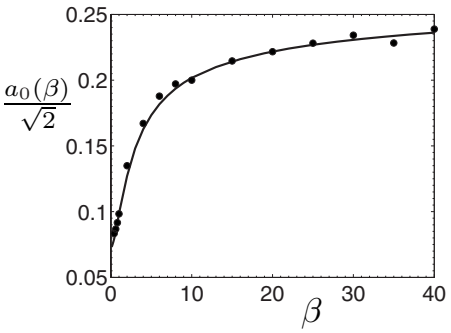

FIG. 3. Graph of $a_0(\beta)/\sqrt{2}$. The solid curve is derived from Eq. (7). The data points are results from Brownian simulations with 10 000 molecules and $\alpha=40$.

As a biological application, we use Eq. (8) to estimate the rate constant of cGMP hydrolysis by an activated PDE molecule in the rod outer segment, which controls the cell hyperpolarization. The rod outer segment can be considered as a cylinder that contains a large number of uniformly distributed disks dividing the space into almost separate compartments that are loosely connected to each other through a narrow gap between the disk perimeters and the outer segment membrane (see Fig. 4) [20,21]. PDE is a diffusible molecule attached to the disk surfaces and becomes activated either spontaneously or after a photon absorption via the phototransduction cascade [20,22]. In its excited conformation PDE hydrolyzes cytoplasmic diffusible cGMP molecules gating the opening of ionic membrane channels, and this hydrolysis is balanced by uniform cGMP synthesis from cytoplasmic GTP. Because cGMP diffuses much faster than PDE (100 $\mu m^2/s^{-1}$ vs 0.8 $\mu m^2/s^{-1}$ [23–25]), we can in first approximation neglect PDE motion [25–27].

Activated PDE hydrolyzes cGMP with high efficiency [28,29], and on average only around one spontaneously activated PDE is present in a single compartment [20,30]. These findings suggest that the rate of cGMP hydrolysis might be controlled by the diffusional encounter rate between cGMP and activated PDE. We shall use our previous results for a narrow domain to estimate the rate constant β_d, which is a fundamental parameter of photoresponse that characterizes cGMP hydrolysis by spontaneous PDE activation in darkness [20,22]. Although this parameter has been measured experimentally, it does any have yet a microscopic definition. We will now derive a molecular expression for β_d that recovers its experimental value. For that purpose, we estimate the steady state flux of diffusing cGMP molecules to an activated PDE site in darkness. Since spontaneous PDE activation occurs uniformly throughout the outer segment, apart from fluctuations, in darkness there is no net cGMP flux between neighboring compartments. This differs from a photon absorption situation, where the exceeding amount of activated PDE converts the affected compartment into a sink for the cGMP concentration. In darkness, at first order, we can neglect the fluxes between the compartments, which is equivalent to introducing a reflecting boundary condition at the rim of each compartment.

Since the rate of cGMP hydrolysis per compartment is inversely proportional to the mean time τ cGMP molecules reach the activated PDE site, we use formula (8) to obtain an

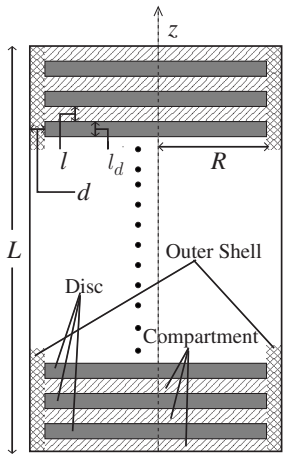

FIG. 4. Geometry of a rod outer segment containing a densely packed stack of parallel disks. A compartment is delimited by two adjacent disks. The compartment height $l\sim 15$ nm is much smaller than the radius R (around a few μm). The width l_d of a disk and the gap d between the disk perimeter and the membrane are both comparable to l. The total length L is around tens of μm.

estimate for this rate. The steady state cGMP flux J_c to an activated PDE site is $J_c=kG_c$, where G_c is the number of cGMP molecules in a compartment and k is [see Eq. (8)]

$$\frac{1}{k}=\tau=\frac{R^2}{D}\left(\pi\frac{l}{a}\frac{a_0(l/a)}{\sqrt{2}}+\frac{4\ln(R/a)-3}{8}\right), \tag{9}$$

where a is the reaction radius, for which we use the sum of the molecular radii of a PDE and cGMP [25–27]. For numerical evaluations, we assume that PDE and cGMP have molecular radii similar to rhodopsin, and we will use $a=3$ nm [25]. To obtain the hydrolysis rate per compartment, we consider the mean number P_c^* of spontaneously activated PDE molecules in a compartment, which can be expressed as a function of the spontaneous PDE activation and deactivation rates μ_+ and μ_- and the PDE surface density ρ: $P_c^*=2\pi R^2\rho\frac{\mu_+}{\mu_-}$ (the factor of 2 accounts for the two disk surfaces attached to a compartment). Because P_c^* is of the order one (see below), the flux J_c is still in the range where it is proportional to P_c^*. Hence, we have $J_c=kP_c^*G_c$. The cumulated hydrolysis rate J_{os} in the whole outer segment is the sum of J_c over all N compartments. Since $G_{os}\approx NG_c$ well approximates the total number of cGMP molecules in the outer segment (the outer shell volume $2\pi RdL$ is negligible compared to the volume πR^2lN of all compartments), we finally obtain

$$J_{os}=kP_c^*G_{os}. \tag{10}$$

From Eqs. (10) and (9) we find for the rate constant β_d

$$\beta_d=kP_c^*=D\frac{2\pi\rho\mu_+}{\mu_-}\frac{8}{8\pi\frac{l}{a}\frac{a_0(l/a)}{\sqrt{2}}+4\ln(R/a)-3}. \tag{11}$$

We conclude that β_d is determined by the mean number of spontaneously activated PDE molecules in a compartment, and not in the outer segment [30]. Furthermore, Eq. (11) shows that β_d depends only logarithmically on the compart-

ment radius R and thus is very similar across species that differ mostly in the radius of the outer segment, in agreement with experimental findings [20].

We now validate our computations by comparing formula (11) with experimental findings. Using data available for toad rods [20,30,31], $\rho=100\ \mu\text{m}^{-1}$, $R=3\ \mu\text{m}$, $\mu_+=4\times10^{-4}\ \text{s}^{-1}$, $\mu_-=1.8\ \text{s}^{-1}$, $D=100\ \mu\text{m}^2/\text{s}^{-1}$, $a=3$ nm, $l=15$ nm, and $\frac{a_0(5)}{\sqrt{2}}=0.17$ [computed using Eq. (7)], we obtain $k=1.9\ \text{s}^{-1}$, $P_c^*=1.26$, and $\beta_d=2.4\ \text{s}^{-1}$. Our prediction for β_d is very close to the experimental value $\beta_d\sim1\ \text{s}^{-1}$ [20]. Moreover, since $k=1.9\ \text{s}^{-1}$ is the catalytic activity of a single activated PDE molecule, our finding is in large contrast to $k=1.6\times10^{-5}\ \text{s}^{-1}$ estimated in [30]. The discrepancy is largely due to the fact that in [30] compartments were not considered, and the outer segment was treated as a homogeneous domain where all activated PDE molecules additively contribute to β_d. In such a homogenized model, each activated PDE molecule was assumed to affect cGMP in the whole outer segment, and therefore the activity of a single molecule needed to fit the experimental value of β_d was largely underestimated. Our derivation shows that, even under uniform conditions in darkness, one has to consider the compartments as fundamental building block.

To conclude, using formula (8), we derived expressions for two key rates of phototransduction: the catalytic activity k of an activated PDE molecule and the dark rate constant β_d. By taking into account the geometrical compartmentalization of the rod outer segment, we found that k is of the order of β_d, and thus $\sim10^5$ times larger than what was estimated assuming a homogeneous outer segment [30]. Our finding has important implications: Since a higher PDE activity leads to larger cGMP fluctuations in a compartment, it should increase the amplitude of the current noise. In addition, one has to analyze the impact of the compartments on the current noise generated by spontaneous PDE activation in darkness. Interestingly, in recent papers [32,33] it was suggested that the dark noise in certain cones is not due to the photopigment instability, as usually believed, but originates from PDE activity. In cones, since activated PDE and ionic channels are located nearby on the same membrane, a high PDE activity may increase the local current fluctuations. In rods, this effect may be less profound, since PDE and the channels are well separated, and diffusion of cGMP acts as a variability suppressor [34]. Hence, a large PDE activity may constitute an important piece in the still unresolved puzzle of why cones are so much noisier compared to rods.

J.R. thanks the FRM Foundation for support. D.H.'s research is supported by an ERC starting grant and HFSP.

[1] R. Zwanzig, Proc. Natl. Acad. Sci. U.S.A. **87**, 5856 (1990).
[2] H. C. Berg and M. Purcell, Biophys. J. **20**, 193 (1977).
[3] G. Wilemski and M. Fixman, J. Chem. Phys. **58**, 4009 (1973).
[4] M. Ward and J. Keller, SIAM J. Appl. Math. **53**, 770 (1993).
[5] M. Ward and E. Van De Velde, IMA J. Appl. Math. **48**, 53 (1992).
[6] I. V. Grigoriev, Y. A. Makhnovskii, A. M. Berezhkovskii, and V. Y. Zitserman, J. Chem. Phys. **116**, 9574 (2002).
[7] D. Holcman and Z. Schuss, J. Stat. Phys. **117**, 975 (2004).
[8] Z. Schuss, A. Singer, and D. Holcman, Proc. Natl. Acad. Sci. U.S.A. **104**, 16098 (2007).
[9] D. Holcman and Z. Schuss, J. Phys. A **41**, 155001 (2008).
[10] A. Singer and Z. Schuss, Phys. Rev. E **74**, 020103(R) (2006).
[11] A. Taflia and D. Holcman, J. Chem. Phys. **126**, 234107 (2007).
[12] J. Bourne and K. Harris, Annu. Rev. Neurosci. **31**, 47 (2008).
[13] K. Klenin, W. Kusnezow, and J. Langowski, J. Chem. Phys. **122**, 214715 (2005).
[14] Z. Schuss, *Theory and Applications of Stochastic Differential Equations*, Wiley Series in Probability and Statistics (Wiley, New York, 1980).
[15] *Handbook of Mathematical Functions*, edited by M. Abramowitz and I. A. Stegun (Dover, New York, 1964).
[16] M. Ward, W. Heshaw, and J. Keller, SIAM J. Appl. Math. **53**, 799 (1993).
[17] A. Singer, Z. Schuss, D. Holcman, and B. Eisenberg, J. Stat. Phys. **122**, 465 (2006).
[18] R. Straube, M. Ward, and M. Falcke, J. Stat. Phys. **129**, 377 (2007).
[19] A. Singer, Z. Schuss, D. Holcman, and B. Eisenberg, J. Stat. Phys. **122**, 437 (2006).
[20] E. Pugh, Jr. and T. Lamb, *Handbook Biological Physics* (Elsevier Science B.V., Amsterdam, 2000), Vol. 3, pp. 183–225.
[21] M. Burns and V. Arshavsky, Neuron **48**, 387 (2005).
[22] E. Pugh, Jr. and T. Lamb, Biochim. Biophys. Acta **1141**, 111 (1993).
[23] Y. Koutalos, K. Nakatani, and K.-W. Yau, Biophys. J. **68**, 373 (1995).
[24] A. Olson and E. Pugh, Jr., Biophys. J. **65**, 1335 (1993).
[25] E. Pugh, Jr. and T. Lamb, J. Physiol. (London) **449**, 719 (1992).
[26] K. R. Naqvi, Chem. Phys. Lett. **28**, 280 (1974).
[27] D. C. Torney and H. M. McConnell, Proc. R. Soc. London, Ser. A **387**, 147 (1983).
[28] I. Leskov, V. Klenchin, J. Handy, G. Whitlock, V. Govardovskii, M. Bownds, T. Lamb, E. Pugh, Jr., and V. Arshavsky, Neuron **27**, 525 (2000).
[29] V. Arshavsky, T. Lamb, and E. Pugh, Jr., Annu. Rev. Physiol. **64**, 153 (2002).
[30] F. Rieke and D. Baylor, Biophys. J. **71**, 2553 (1996).
[31] R. Hamer, S. Nicholas, D. Tranchina, T. Lamb, and J. Jarvinen, Visual Neurosci. **22**, 417 (2005).
[32] D. Holcman and J. Korenbrot, J. Gen. Physiol. **125**, 641 (2005).
[33] Y. Fu, V. Kefalov, D. Luo, T. Xue, and K. Yau, Nat. Neurosci. **11**, 565 (2008).
[34] P. Bisegna, G. Caruso, D. Andreucci, L. Shen, V. Gurevich, H. Hamm, and E. DiBenedetto, Biophys. J. **94**, 3363 (2008).